

## Supporting Information for

# Vibrational Perturbation of the [FeFe] Hydrogenase H-Cluster Revealed by $^{13}\text{C}^2\text{H}$ -ADT Labeling

Vladimir Pelmeshnikov,<sup>†</sup> James A. Birrell,<sup>\*,‡</sup> Leland B. Gee,<sup>§</sup> Casseday P. Richers,<sup>||</sup> Edward J. Reijerse,<sup>‡</sup> Hongxin Wang,<sup>⊥</sup> Simon Arragain,<sup>#,∇</sup> Nakul Mishra,<sup>∇</sup> Yoshitaka Yoda,<sup>°</sup> Hiroaki Matsuura,<sup>♦</sup> Lei Li,<sup>¶</sup> Kenji Tamasaku,<sup>■</sup> Thomas B. Rauchfuss,<sup>\*,||</sup> Wolfgang Lubitz,<sup>‡</sup> and Stephen P. Cramer<sup>\*,⊥</sup>

<sup>†</sup>Institut für Chemie, Technische Universität Berlin, 10623 Berlin, Germany

<sup>‡</sup>Max Planck Institute for Chemical Energy Conversion, 45470 Mülheim an der Ruhr, Germany

<sup>§</sup>Department of Chemistry, Stanford University, Stanford, California 94305, United States

<sup>||</sup>School of Chemical Sciences, University of Illinois, Urbana, Illinois 61801, United States

<sup>⊥</sup>SETI Institute, Mountain View, California 94043, United States

<sup>#</sup>IFP Energies nouvelles, 92852 Rueil-Malmaison, France

<sup>∇</sup>Department of Chemistry, University of California, Davis, California 95616, United States

<sup>°</sup>Precision Spectroscopy Division, SPring-8/JASRI, Sayo, Hyogo 679-5198, Japan

<sup>♦</sup>Life Science Research Infrastructure Group, Advanced Photon Technology Division, RIKEN/SPring-8 Center, Sayo, Hyogo 679-5148, Japan

<sup>¶</sup>Hyogo Science and Technology Association, Synchrotron Radiation Research Center, Tatsuno-shi, Hyogo 679-5165, Japan

<sup>■</sup>Research and Utilization Division, SPring-8/JASRI, Sayo, Hyogo 679-5198, Japan

\* Corresponding Authors

## Materials and Methods

**Synthesis of  $^{12}\text{CH-ADT}$  and  $^{13}\text{CD-ADT}$  Precursor Complex.** We recently reported a new simplified synthesis for a triply labeled  $[\text{2Fe}]_{\text{H}}$  precursor complex  $(\text{Et}_4\text{N})_2[^{57}\text{Fe}_2(\text{S}^{13}\text{C}^2\text{H}_2)_2\text{NH}](\text{CN})_2(\text{CO})_4 = ^{13}\text{CD-1}$ .<sup>1</sup>  $^{13}\text{CD-1}$  and its  $^{57}\text{Fe}$ -only labeled analogue  $(\text{Et}_4\text{N})_2[^{57}\text{Fe}_2(\text{S}^{12}\text{C}^1\text{H}_2)_2\text{NH}](\text{CN})_2(\text{CO})_4 = \mathbf{1}$  were synthesized as previously described.<sup>1</sup>

**Preparation of *CrHydA1* for NRVS and FTIR Spectroscopy.** *CrHydA1* was produced recombinantly in *Escherichia coli* and artificially matured with precursor complexes  $\mathbf{1}$  and  $^{13}\text{CD-1}$  as described previously.<sup>2</sup> NRVS samples (5 mM) were prepared in the  $\text{H}_{\text{hyd}}$  state by reduction with 100 mM sodium dithionite at pH 6 (in 50 mM MES, 50 mM HEPES, 300 mM KCl, pH 6) under an atmosphere of 2%  $\text{H}_2$ . The *CrHydA1*  $\text{H}_{\text{ox}}$  sample was prepared in the same buffer, by incubation under nitrogen in the absence of additional reductants. NRVS cells were filled with 40  $\mu\text{L}$  of sample and frozen in liquid nitrogen, and 10  $\mu\text{L}$  were transferred to an FTIR cell, between two  $\text{CaF}_2$  windows (20 mm x 4 mm, Korth Kristalle, Altenholz) separated with a 50  $\mu\text{m}$  Teflon spacer coated with vacuum grease and closed with rubber rings. The temperature of the cell was maintained at 25  $^\circ\text{C}$  using a water circulator system (Huber, Offenburg). Spectra were measured on a Bruker IFS 66v/S FTIR spectrometer equipped with a nitrogen cooled Bruker mercury cadmium telluride (MCT) detector. Spectra were collected in the double-sided, forward-backward mode with a resolution of 2  $\text{cm}^{-1}$ , an aperture setting of 1.5 mm and a scan velocity of 20 Hz. Spectra are the average of 1000 scans. Data were processed using home-written routines in the MATLAB<sup>TM</sup> environment.

**NRVS Measurements and Processing.** Nuclear resonance vibrational spectroscopy measurements of the  $(^{13}\text{CD-1})$  precursor and  $(^{13}\text{CD-1})$ -*CrHydA1*  $\text{H}_{\text{hyd}}$  samples were conducted at SPring-8 BL19LXU.<sup>3</sup> A liquid  $\text{N}_2$ -cooled Si (111) high heat load monochromator was used to produce an incident beam with  $\sim 1.0$  eV resolution, followed by a high resolution monochromator [Ge (331) x Si (975) crystals] to achieve a  $\sim 0.8$  meV ( $6.5 \text{ cm}^{-1}$ ) energy resolution at 14.4125 keV.<sup>4</sup> The use of a 25 m undulator at BL19LXU afforded  $6.5 \times 10^9$  photons  $\text{s}^{-1}$ .<sup>5</sup> {Hara, 2002 #7844} During NRVS measurements, the samples were maintained at cryogenic temperature using a liquid He cryostat. The real sample temperatures, derived from anti-Stokes / Stokes intensity ratios, were 45-60 K. A 4-channel avalanche photodiode detector (APD) array was used to detect the delayed nuclear fluorescence and the  $\text{K}\alpha$  fluorescence following nuclear excitation of  $^{57}\text{Fe}$  atoms. The spectra were recorded with a step size of 0.27 meV.

The raw NRVS data were analyzed by the PHOENIX software package<sup>6</sup> executed through spectra.tools,<sup>7</sup> yielding  $^{57}\text{Fe}$  partial density of vibrational states ( $^{57}\text{Fe-PVDOS}$ ). The resonance peak position for each scan was aligned in the analysis, and the energy was calibrated periodically with a standard sample of  $\text{NEt}_4^{57}\text{FeCl}_4$  with a prominent peak at  $380 \text{ cm}^{-1}$ . The ADT-labeled  $^{13}\text{CD-1-CrHydA1}$   $\text{H}_{\text{hyd}}$  samples were measured in 4 beamtimes with 90 total scans in 5 datasets while the regular  $\mathbf{1-CrHydA1}$   $\text{H}_{\text{hyd}}$  samples were measured in 5 beamtimes with 125 total scans in 6 datasets. There were two pairs of  $(^{13}\text{CD-1})$ -*CrHydA1* datasets where an *in-situ* energy calibration was performed with a  $^{57}\text{Fe}$  powder sample measured at a room temperature stage outside the sample chamber. Those scans were individually calibrated before using the analysis software PHOENIX. However, we did not find any obvious difference between the *in-situ* calibrated and regular periodically calibrated datasets.

The scans were divided into segments with very different collection times with respect to energy regions. In this study, the acquisition time for every data point in the region of interest (*i.e.* from 640 to 830  $\text{cm}^{-1}$ , X–Fe–H related bending region) was 30 seconds/point (s/p), in the middle region of 400 to 640  $\text{cm}^{-1}$  (Fe–CO and Fe–CN) was 6 s/p, and that for the front region of -240  $\text{cm}^{-1}$  to 400  $\text{cm}^{-1}$  was 1 s/p. For the two pairs of *in-situ* calibrated datasets, the acquisition time for the X–Fe–H bending region (*from* 640 to 830  $\text{cm}^{-1}$ ) was still 30 s/p. However, as the  $^{57}\text{Fe}$  powder peaks and the nuclear resonant regions need to be well captured, the -90 to 90  $\text{cm}^{-1}$  region used 2 s/p while the 215 to 355  $\text{cm}^{-1}$  region used 10 s/p.

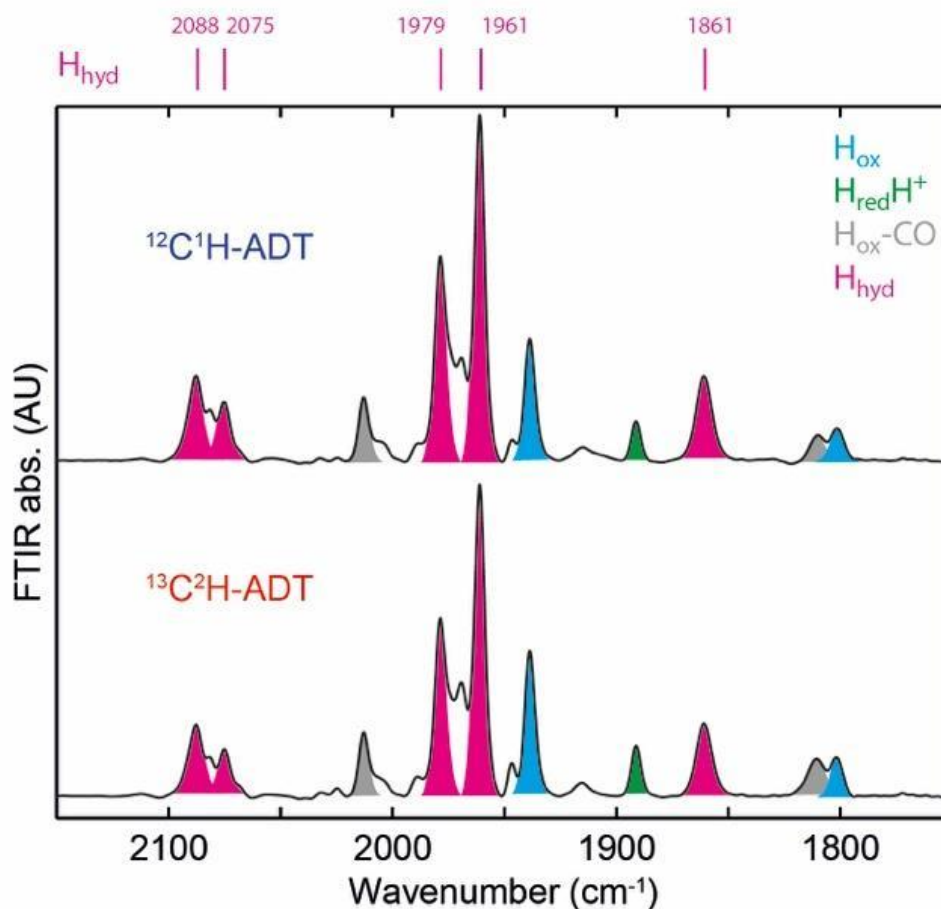
The *CrHydA1*  $\text{H}_{\text{ox}}$  sample was measured at P01, PETRA-III, Hamburg.<sup>8</sup> The experimental setup established at the beamline including a two-step monochromatization (energy resolution of  $\sim 1$  meV) and detection by avalanche photo diodes was used. Sample, in home-built copper sample holder, was positioned in the beam on the top of a closed cycle helium cryostat with a copper cold finger, using a home-built copper adapter. The sample was then covered with a mylar cylinder and a metal cover. The temperature at the base of the sample was maintained at 10 K and the Stokes/anti-Stokes imbalance derived real sample temperatures were 10–20 K. NRVS spectral analysis was performed using routines written in Python. The experimentally determined  $^{57}\text{Fe}$ -PVDOS was calculated with a binning of 0.5 meV.

**DFT Calculations.** Initial coordinates for the density functional theory (DFT) modeling of the precursor complex  $(\text{Et}_4\text{N})_2[\text{Fe}_2[(\text{SCH}_2)_2\text{NH}](\text{CN})_2(\text{CO})_4] = \mathbf{1}$  were based on its crystallographic characterization.<sup>9</sup> The  $\text{Et}_4\text{N}^+$  counterions were omitted in the calculations, leading to the anionic  $[\text{Fe}_2[(\text{SCH}_2)_2\text{NH}](\text{CN})_2(\text{CO})_4]^{2-}$  monomolecular species. The protein  $\text{H}_{\text{hyd}}$  and  $\text{H}_{\text{ox}}$  models were based on the 1.73 Å resolution 5BYQ X-ray data for the semisynthetic *Clostridium pasteurianum* [FeFe] hydrogenase (*CpI*) matured with the ODT variant of the  $[\text{2Fe}]_{\text{H}}$  subcluster (*CpI*<sup>ODT</sup>).<sup>10</sup> To account for the presently relevant *CrHydA1* species, only a single side chain S232 (*CpI*) had to be modified to A94 (*CrHydA1*). This approach is equivalent to the H-cluster DFT model construction applied by some of us earlier<sup>11–13</sup> for studying states  $\text{H}_{\text{hyd}}$ ,  $\text{H}_{\text{sred}}\text{H}^+$ , and  $\text{H}_{\text{red}}\text{H}^+$ . Denoted as *L'* (*Large prime*), this molecular system includes the (i)  $[\text{2Fe}]_{\text{H}}$  subcluster, (ii) its immediate protein environment, and (iii) the  $[\text{4Fe–4S}]_{\text{H}}$  subcluster. All the  $13 \times \text{C}_\alpha$  carbon nuclei of the *L'* model were locked to their original X-ray crystallographically defined positions during structure optimizations.<sup>14</sup>

The molecular geometry optimizations, as well as subsequent normal mode analyses, were performed using GAUSSIAN 09 Revision D.01<sup>15</sup> based on the densities exported from single point calculations performed by JAGUAR 9.4<sup>16</sup> that provided a high-quality initial guess for the starting (non-optimized) structures. The PBE0<sup>17–18</sup> hybrid functional and the LACV3P\*\* basis set (as implemented in JAGUAR) were employed. For the first- and second-row elements, LACV3P\*\* implies 6-311G\*\* triple- $\zeta$  basis sets including polarization functions. For the Fe atoms, LACV3P\*\* consists of a triple- $\zeta$  basis set for the outermost core and valence orbitals, and the quasi-relativistic Los Alamos effective core potential (ECP) for the innermost electrons. The molecular systems environment was considered using a self-consistent reaction field (SCRf) polarizable continuum model and integral equation formalism (IEF-PCM)<sup>19</sup> as implemented in GAUSSIAN 09, with the static dielectric constant set to  $\epsilon = 4.0$  as often used for proteins, and the remaining IEF-PCM parameters at their default values for water. The computational scheme for the protein models furthermore included two-body D3 empirical dispersion correction by Grimme *et al.* in its original formulation.<sup>20</sup> The H-cluster redox states

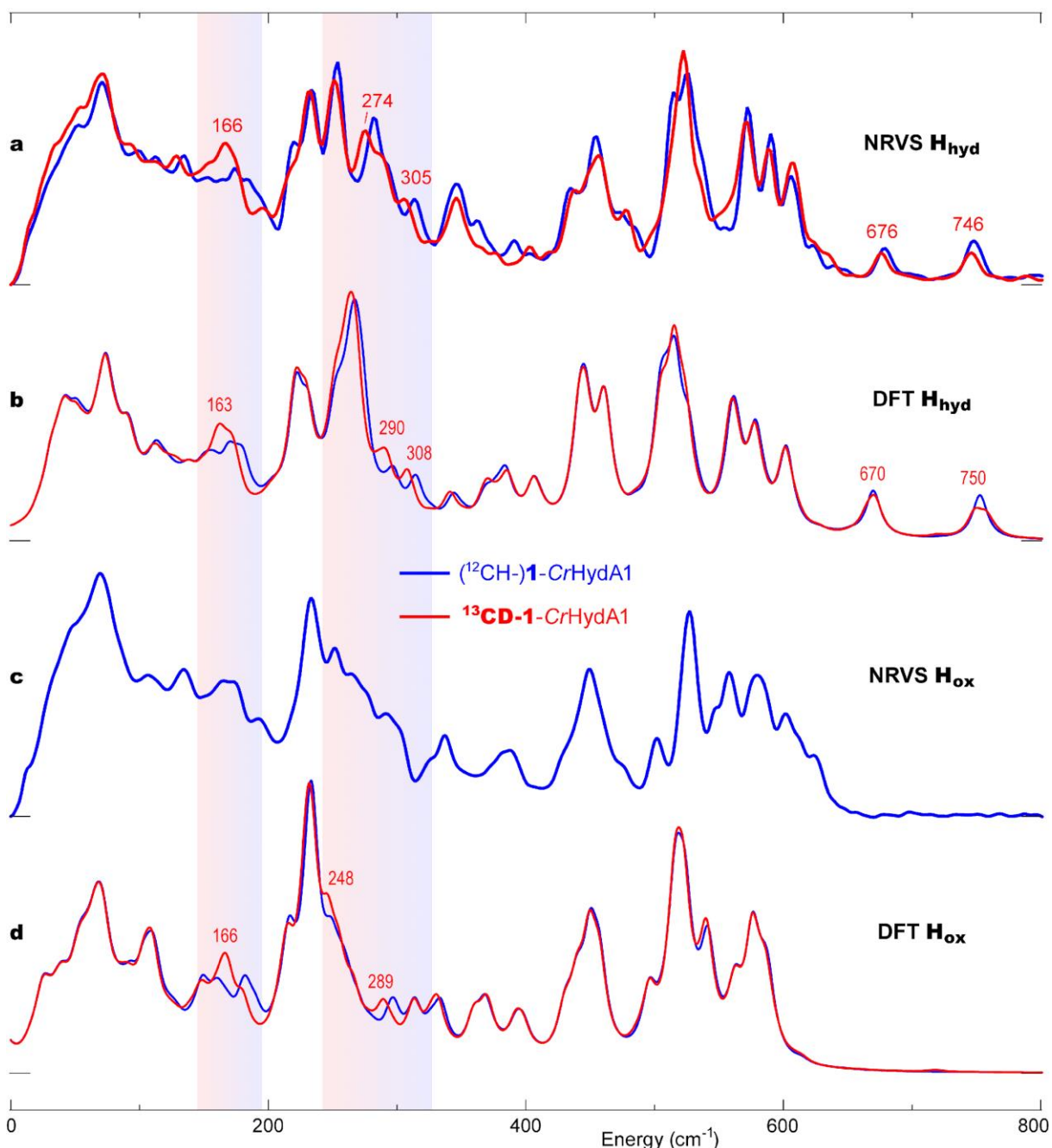
$[4\text{Fe-4S}]_{\text{H}^+}\text{-Fe}_p(\text{II})\text{Fe}_d(\text{II})$  and  $[4\text{Fe-4S}]_{\text{H}^{2+}}\text{-Fe}_p(\text{II})\text{Fe}_d(\text{I})$ , correspondingly, were confirmed for the electronic configurations of the present  $\text{H}_{\text{hyd}}$  and  $\text{H}_{\text{ox}}$  models.

The  $^{57}\text{Fe}$ -PVDOS intensities and internuclear displacements were extracted from normal mode outputs using an in-house Q-SPECTOR program tool, successfully applied by us to simulate the [FeFe] hydrogenase<sup>11-13, 21</sup> and other molecular systems' NRVS spectra. To empirically account for experimental NRVS lineshapes of the  $(^{13}\text{CD-})\mathbf{1}$  /  $(^{13}\text{CD-})\mathbf{1-CrHydA1}$  samples, the DFT-computed  $^{57}\text{Fe}$ -PVDOS intensities were correspondingly broadened by convolution with a full width at half maximum (FWHM) = 12 / 14  $\text{cm}^{-1}$  Lorentzian; homogeneous empirical scaling by 96% / 94% was applied to the calculated frequencies > 350 / 400  $\text{cm}^{-1}$ .



## Supplementary Figures

**Figure S1.** FTIR spectra of the ( $^{12}\text{CH}$ )-**1-CrHydA1** (top) and  $^{13}\text{CD}$ -**1-CrHydA1** (bottom) samples poised in the  $\text{H}_{\text{hyd}}$  state. Bands from the  $\text{H}_{\text{hyd}}$  state are colored purple. Bands of smaller intensity from the additional states  $\text{H}_{\text{ox}}$ ,  $\text{H}_{\text{red}}\text{H}^+$  and  $\text{H}_{\text{ox}}\text{-CO}$  are colored blue, green, and gray, respectively. From the relative intensity of the CO stretch at  $1961\text{ cm}^{-1}$  in the  $\text{H}_{\text{hyd}}$  state vs. the equivalent  $\text{H}_{\text{ox}}$  band at  $1940\text{ cm}^{-1}$ , we estimate that  $\sim 80\%$  of the samples were in the  $\text{H}_{\text{hyd}}$  state for **1-CrHydA1** and  $\sim 70\%$  in  $^{13}\text{CD}$ -**1-CrHydA1**. Obtaining pure  $\text{H}_{\text{hyd}}$  spectra is challenging as  $\text{H}_{\text{hyd}}$  is a rather unstable intermediate that decays with time and can only be captured under specific conditions (low pH and high amounts of reductant). There is always a contribution from a few additional states due to reoxidation of  $\text{H}_{\text{hyd}}$  (giving  $\text{H}_{\text{ox}}$ ) or degradation of the H-cluster (producing  $\text{H}_{\text{ox}}\text{-CO}$  through “cannibalization”). Note that NRVS samples were frozen at the same time as IR samples were prepared, but there is a small delay 5-10 min before the IR samples are measured. Thus, the true proportion of  $\text{H}_{\text{hyd}}$  is likely to be higher in the NRVS samples. The contribution from other states to the NRVS spectrum will be small and certainly not responsible for the large isotope dependent changes we report in the current manuscript. In particular,  $\text{H}_{\text{hyd}}$  is the only state so far



identified with peaks in the 650 – 750  $\text{cm}^{-1}$  region of the NRVS spectrum and so changes in this region are entirely from  $\text{H}_{\text{hyd}}$ .

**Figure S2.**  $^{57}\text{Fe}$ -PVDOS for the [FeFe] hydrogenase  $\text{H}_{\text{hyd}}$  /  $\text{H}_{\text{ox}}$  state isotopologues ( $^{12}\text{CH-}$ )1-CrHydA1 (blue) vs.  $^{13}\text{CD-}$ 1-CrHydA1 (red) from (a) / (c) NRVS experiment and (b) / (d) DFT calculations, correspondingly; the  $^{13}\text{CD-}$ 1-CrHydA1 NRVS data availability is limited to the  $\text{H}_{\text{hyd}}$  sample. Notable isotope-dependent spectral features unique to the  $^{13}\text{CD-}$ 1-CrHydA1 species are marked with their vibrational energies (numbers shown in red). Regions displaying consistent  $^{12}\text{CH-}$ -vs- $^{13}\text{CD}$  ADT spectral shifts (in a, b, and d) are highlighted using vertical semi-transparent bars.

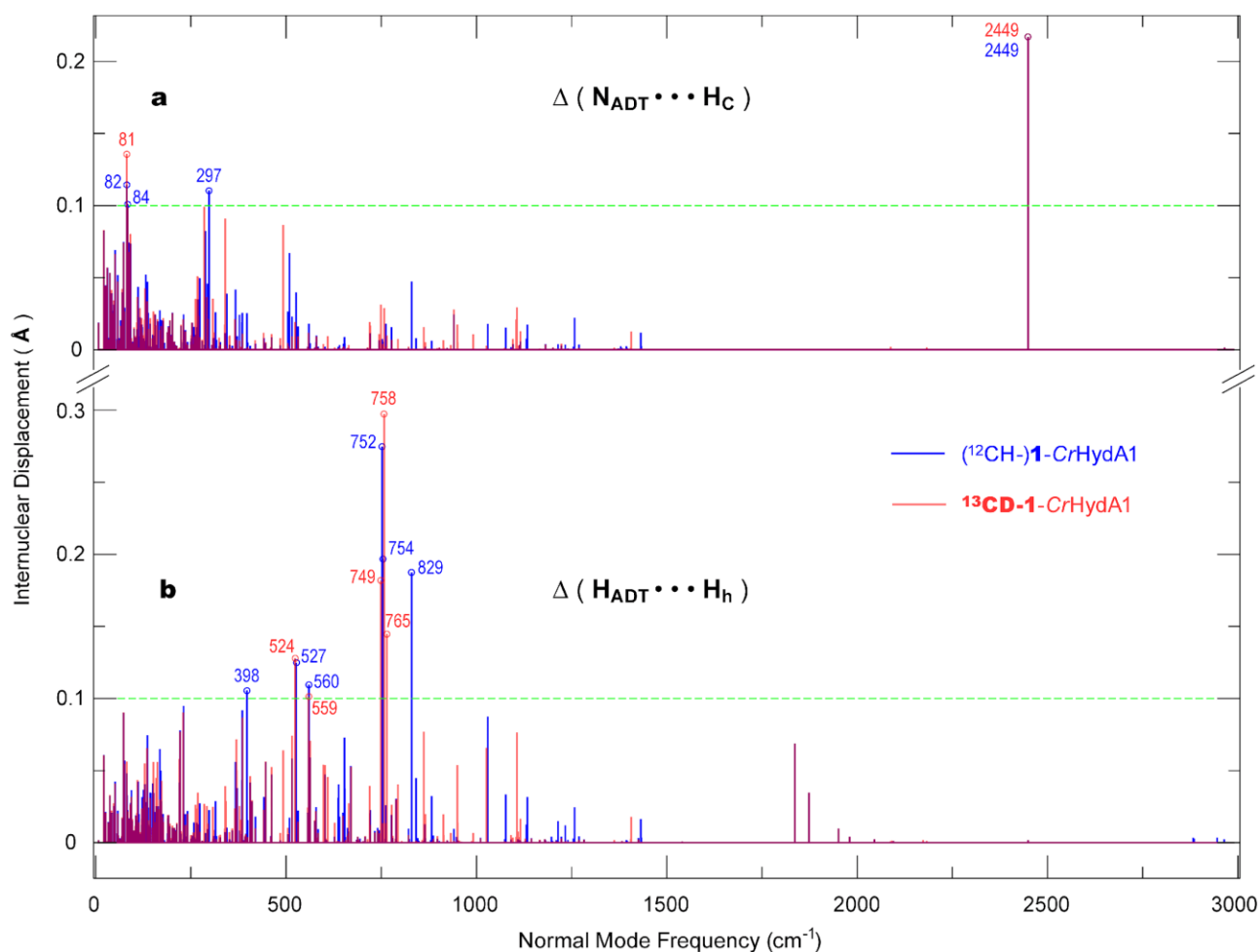


**Figure S3.** Relative displacement amplitudes in the nuclei pairs (a)  $N_{ADT} \cdots H_C$  and (b)  $H_{ADT} \cdots H_h$  (as designated in **Figure 1b**) from the  $\mathbf{1}\text{-CrHydA1}$  (blue) and  $^{13}\text{CD}\mathbf{-1}\text{-CrHydA1}$  (red)  $H_{hyd}$  state DFT models across the entire vibrational spectra. Normal modes with significant internuclear displacements ( $>0.1 \text{ \AA}$  cut-off shown as green broken line) of the types (a) and (b) are labeled with their frequencies, listed in **Table S1**, and provided as animations as part of the **Supporting Information**.

## Supplementary Tables

**Table S1.** Normal modes with significant ( $>0.1$  Å) relative displacement amplitudes in the nuclei pairs  $\text{H}_{\text{ADT}}\cdots\text{H}_{\text{h}}$  and  $\text{N}_{\text{ADT}}\cdots\text{H}_{\text{C}}$  (as designated in **Figure 1b**) from the **1-CrHydA1** and  **$^{13}\text{CD-1-CrHydA1}$**   $\text{H}_{\text{hyd}}$  state DFT models. Animated representations of these vibrational modes are provided as a separate part of the **Supporting Information**.

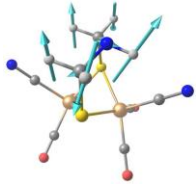
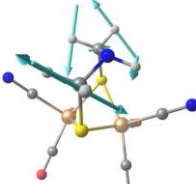
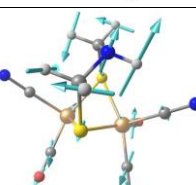
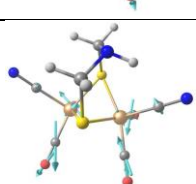
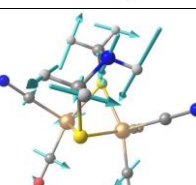
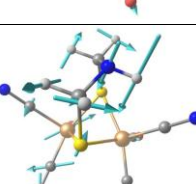
$\text{H}_{\text{ADT}}\cdots\text{H}_{\text{h}}$ (= 2.06 Å) <sup>a</sup>				$\text{N}_{\text{ADT}}\cdots\text{H}_{\text{C}}$ (= 2.26 Å) <sup>a</sup>			
<b>1-CrHydA1</b>		<b><math>^{13}\text{CD-1-CrHydA1}</math></b>		<b>1-CrHydA1</b>		<b><math>^{13}\text{CD-1-CrHydA1}</math></b>	
Frequency ( $\text{cm}^{-1}$ )	Displacement <sup>b</sup> (Å)	Frequency ( $\text{cm}^{-1}$ )	Displacement <sup>b</sup> (Å)	Frequency ( $\text{cm}^{-1}$ )	Displacement <sup>b</sup> (Å)	Frequency ( $\text{cm}^{-1}$ )	Displacement <sup>b</sup> (Å)
398	0.106	<b>524</b>	<b>0.128</b>	82	0.115	<b>81</b>	<b>0.136</b>
527	0.125	<b>559</b>	<b>0.102</b>	84	0.101	<b>2449</b>	<b>0.217</b>
560	0.110	<b>749</b>	<b>0.182</b>	297	0.110		
752	0.275	<b>758</b>	<b>0.297</b>	2449	0.217		
754	0.197	<b>765</b>	<b>0.145</b>				
829	0.187						

<sup>a</sup> Optimized internuclear distance.

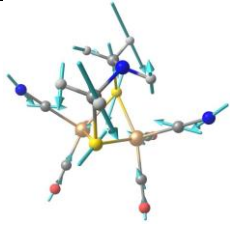
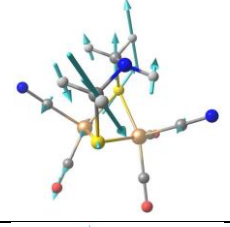
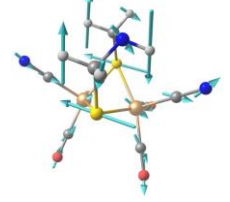
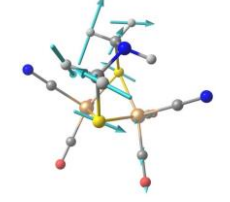
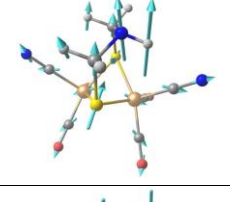
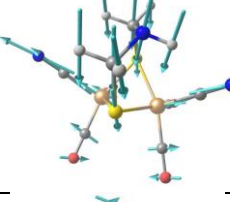
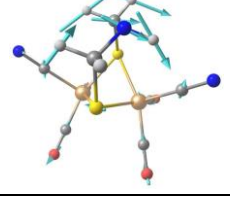
<sup>b</sup> The corresponding internuclear distance contraction is approximately 50% of the displacement amplitude.



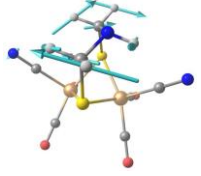
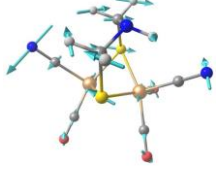
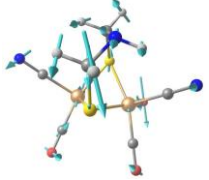
**Table S2.** [2Fe]<sub>H</sub> precursor vibrational modes summary from the (<sup>12</sup>CH-)1 and <sup>13</sup>CD-1 DFT models. Animated representations of selected vibrational modes are provided as a separate part of the **Supporting Information**.

Mode atomic motions	Frequency <b>1</b> (cm <sup>-1</sup> )	Frequency <b><sup>13</sup>CD-1</b> (cm <sup>-1</sup> )	Difference <b>1 - <sup>13</sup>CD-1</b> (cm <sup>-1</sup> )	Characterization
	1058/902	<b>769/734</b>	289/168	In-phase bending/rotation of the -CH <sub>2</sub> - groups, admixed with ADT amine proton motion parallel to the mirror symmetry plane of <b>1</b> .
	848	<b>674</b>	174	Out-of-phase bending/rotation of the -CH <sub>2</sub> - groups, admixed with ADT amine proton motion perpendicular to the mirror symmetry plane of <b>1</b> .
	534	<b>530</b>	4	ADT motion coupled to the CO bending/stretching.
	518	<b>518</b>	0	Similar to 534/ <b>530</b> but negligible ADT motion, hence no isotope shift.
	508	<b>492</b>	16	Similar to 534/ <b>530</b> but with a different phase of CO/ADT motions, and different CN motion.
	506	<b>489</b>	17	Similar to 508 but with larger contribution of the Fe <sub>p</sub> -bound CO bending, and smaller contribution of the Fe <sub>d</sub> -bound CO bending.

( Table continued on the next page )

	326	<b>329/314</b>	-3/12	Fe–S motion coupled to CO and CN movement and ADT “flapping”. <b>329</b> has much less CO/CN motion and does not show the “flapping”. <b>314</b> is like 329 but with less CO/CN/FeS motion.
	292	<b>287</b>	5	ADT fragment wagging/rotation between 2xFe. Similar for ( <sup>12</sup> CH-) <b>1</b> and <sup>13</sup> CD- <b>1</b> .
	286	<b>285</b>	1	ADT fragment bending/rocking between 2xFe. Similar for ( <sup>12</sup> CH-) <b>1</b> and <sup>13</sup> CD- <b>1</b> .
	272	<b>264</b>	8	Independent S movement with Fe side-to-side motion. Again, very similar for ( <sup>12</sup> CH-) <b>1</b> and <sup>13</sup> CD- <b>1</b> .
	225	<b>224</b>	1	Fe <sub>2</sub> S <sub>2</sub> unit flattening, out of phase with the ADT movement.
	203	<b>201</b>	2	Fe <sub>2</sub> S <sub>2</sub> unit flattening but in phase with ADT movement.
	173	<b>168</b>	5	Rocking of the –H <sub>2</sub> C-NH-CH <sub>2</sub> – assembly / Seesaw motion of the Fe <sub>2</sub> S <sub>2</sub> unit.

( Table continued on the next page )

	160	<b>143</b>	17	Out-of-phase rotation of the two ADT –μSCH <sub>2</sub> – groups around their S–C axes.
	129	<b>127</b>	2	In-phase rotation of the two ADT –μSCH <sub>2</sub> – groups / Fe <sub>2</sub> S <sub>2</sub> swivel motion.
	105	<b>104</b>	1	ADT fragment wagging/rotation between 2xFe, as well involving CO/CN ligands.

## Supplementary References

1. Reijerse, E. J.; Pelmeshnikov, V.; Birrell, J. A.; Richers, C. P.; Kaupp, M.; Rauchfuss, T. B.; Cramer, S. P.; Lubitz, W., Asymmetry in the Ligand Coordination Sphere of the [FeFe] Hydrogenase Active Site Is Reflected in the Magnetic Spin Interactions of the Aza-propanedithiolate Ligand. *J. Phys. Chem. Lett.* **2019**, *10*, 6794-6799.
2. Esselborn, J.; Lambertz, C.; Adamska-Venkatesh, A.; Simmons, T.; Berggren, G.; Noth, J.; Siebel, J.; Hemschemeier, A.; Artero, V.; Reijerse, E.; Fontecave, M.; Lubitz, W.; Happe, T., Spontaneous activation of [FeFe]-hydrogenases by an inorganic [2Fe] active site mimic. *Nat. Chem. Biol.* **2013**, *9* (10), 607-9.
3. Yabashi, M.; Mochizuki, T.; Yamazaki, H.; Goto, S.; Ohashi, H.; Takeshita, K.; Ohata, T.; Matsushita, T.; Tamasaku, K.; Tanaka, Y.; Ishikawa, T., Design of a beamline for the SPring-8 long undulator source 1. *Nucl. Inst. Meth. A* **2001**, *467*, 678-681.
4. Yoda, Y.; Yabashi, M.; Izumi, K.; Zhang, X. W.; Kishimoto, S.; Kitao, S.; Seto, M.; Mitsui, T.; Harami, T.; Imai, Y.; Kikuta, S., Nuclear resonant scattering beamline at SPring-8. *Nucl. Inst. Meth. A* **2001**, *467*, 715-718.
5. Hara, T.; Yabashi, M.; Tanaka, T.; Bizen, T.; Goto, S.; Marechal, X. M.; Seike, T.; Tamasaku, K.; Ishikawa, T.; Kitamura, H., The brightest x-ray source: A very long undulator at SPring-8. *Rev. Sci. Instrum.* **2002**, *73* (3), 1125-1128.
6. Sturhahn, W., CONUSS and PHOENIX: evaluation of nuclear resonant scattering data. *Hyp. Int.* **2000**, *125*, 149-172.
7. Gee, L. B. [www.spectra.tools](http://spectra.tools): NRVS Spectra Processing Tool. [http://spectra.tools/cgi-bin/controller.pl?body=NRVS\\_Tool](http://spectra.tools/cgi-bin/controller.pl?body=NRVS_Tool).
8. Wille, H.-C.; Franz, H.; Röhlberger, R.; Caliebe, W. A.; Dill, F.-U., Nuclear resonant scattering at PETRA III : Brilliant opportunities for nano – and extreme condition science. *J. Phys.: Conf. Ser.* **2010**, *217*, 012008.

9. Li, H. X.; Rauchfuss, T. B., Iron carbonyl sulfides, formaldehyde, and amines condense to give the proposed azadithiolate cofactor of the Fe-only hydrogenases. *J. Am. Chem. Soc.* **2002**, *124* (5), 726-727.
10. Esselborn, J.; Muraki, N.; Klein, K.; Engelbrecht, V.; Metzler-Nolte, N.; Apfel, U.-P.; Hofmann, E.; Kurisu, G.; Happe, T., A structural view of synthetic cofactor integration into [FeFe]-hydrogenases. *Chem. Sci.* **2015**, *7*, 959-968.
11. Pham, C. C.; Mulder, D. W.; Pelmeshnikov, V.; King, P. W.; Ratzloff, M. W.; Wang, H.; Mishra, N.; Alp, E. E.; Zhao, J.; Hu, M. Y.; Tamasaku, K.; Yoda, Y.; Cramer, S. P., Terminal Hydride Species in [FeFe]-Hydrogenases Are Vibrationally Coupled to the Active Site Environment. *Angew. Chem., Int. Ed.* **2018**, *57* (33), 10605-10609.
12. Pelmeshnikov, V.; Birrell, J. A.; Pham, C. C.; Mishra, N.; Wang, H. X.; Sommer, C.; Reijerse, E.; Richers, C. P.; Tamasaku, K.; Yoda, Y.; Rauchfuss, T. B.; Lubitz, W.; Cramer, S. P., Reaction Coordinate Leading to H<sub>2</sub> Production in [FeFe]-Hydrogenase Identified by Nuclear Resonance Vibrational Spectroscopy and Density Functional Theory. *J. Am. Chem. Soc.* **2017**, *139* (46), 16894-16902.
13. Birrell, J. A.; Pelmeshnikov, V.; Mishra, N.; Wang, H. X.; Yoda, Y.; Tamasaku, K.; Rauchfuss, T. B.; Cramer, S. P.; Lubitz, W.; DeBeer, S., Spectroscopic and Computational Evidence that [FeFe] Hydrogenases Operate Exclusively with CO-Bridged Intermediates. *J. Am. Chem. Soc.* **2020**, *142* (1), 222-232.
14. Pelmeshnikov, V.; Blomberg, M. R. A.; Siegbahn, P. E., A theoretical study of the mechanism for peptide hydrolysis by thermolysin. *J. Biol. Inorg. Chem.* **2002**, *7* (3), 284-298.
15. Frisch, M. J.; Trucks, G. W.; Schlegel, H. B.; Scuseria, G. E.; Robb, M. A.; Cheeseman, J. R.; Scalmani, G.; Barone, V.; Mennucci, B.; Petersson, G. A.; Nakatsuji, H.; Caricato, M.; Li, X.; Hratchian, H. P.; Izmaylov, A. F.; Bloino, J.; Zheng, G.; Sonnenberg, J. L.; Hada, M.; Ehara, M.; Toyota, K.; Fukuda, R.; Hasegawa, J.; Ishida, M.; Nakajima, T.; Honda, Y.; Kitao, O.; Nakai, H.; Vreven, T.; Montgomery, J. A., Jr.; Peralta, J. E.; Ogliaro, F.; Bearpark, M.; Heyd, J. J.; Brothers, E.; Kudin, K. N.; Staroverov, V. N.; Kobayashi, R.; Normand, J.; Raghavachari, K.; Rendell, A.; Burant, J. C.; Iyengar, S. S.; Tomasi, J.; Cossi, M.; Rega, N.; Millam, J. M.; Klene, M.; Knox, J. E.; Cross, J. B.; Bakken, V.; Adamo, C.; Jaramillo, J.; Gomperts, R.; Stratmann, R. E.; Yazyev, O.; Austin, A. J.; Cammi, R.; Pomelli, C.; Ochterski, J. W.; Martin, R. L.; Morokuma, K.; Zakrzewski, V. G.; Voth, G. A.; Salvador, P.; Dannenberg, J. J.; Dapprich, S.; Daniels, A. D.; Farkas, Ö.; Foresman, J. B.; Ortiz, J. V.; Cioslowski, J.; Fox, D. J., Gaussian 09 Rev D.01. *Gaussian 09, Revision D.01, Gaussian Inc., Wallingford CT, 2009.*
16. Jaguar, Version 9.4, Schrodinger, Inc., New York, NY, 2016.
17. Adamo, C.; Barone, V., Toward reliable density functional methods without adjustable parameters: The PBE0 model. *J. Chem. Phys.* **1999**, *110* (13), 6158-6170.
18. Perdew, J. P.; Burke, K.; Ernzerhof, M., Generalized gradient approximation made simple. *Phys. Rev. Lett.* **1996**, *77* (18), 3865-3868.
19. Tomasi, J.; Mennucci, B.; Cammi, R., Quantum mechanical continuum solvation models. *Chem. Rev.* **2005**, *105* (8), 2999-3093.
20. Grimme, S.; Antony, J.; Ehrlich, S.; Krieg, H., A consistent and accurate *ab initio* parametrization of density functional dispersion correction (DFT-D) for the 94 elements H-Pu. *J. Chem. Phys.* **2010**, *132* (15), 154104.
21. Reijerse, E. J.; Pham, C. C.; Pelmeshnikov, V.; Gilbert-Wilson, R.; Adamska-Venkatesh, A.; Siebel, J. F.; Gee, L. B.; Yoda, Y.; Tamasaku, K.; Lubitz, W.; Rauchfuss, T. B.; Cramer, S. P., Direct observation of an iron bound terminal hydride intermediate in [FeFe] hydrogenase. *J. Am. Chem. Soc.* **2017**, *139* (12), 4306-4309.